19th Australasian Fluid Mechanics Conference
Melbourne, Australia
8-11 December 2014

Reconstruction of Turbulent Pipe Flow using Resolvent Modes: Application to Low-order Models and Flow Control

F. Gómez[1],H. M. Blackburn[1], M. Rudman[1], A. S. Sharma[2] and B. J. McKeon[3]

[1]Department of Mechanical and Aerospace Engineering
Monash University, Victoria 3800, Australia

[2]Faculty of Engineering and the Environment
University of Southampton, Southampton SO17 1BJ, UK

[3]Graduate Aerospace Laboratories
California Institute of Technology, Pasadena, CA 91125, USA

Abstract

A novel energy-based reduced-order model with the ability of isolating specific dynamics in turbulent pipe flow is investigated. The methodology to construct the model is discussed in detail, highlighting the limitations of the approach and future directions. Present results open up a new possibility for representing turbulent flows and performing flow control studies.

Introduction

Reduced-order models able to represent turbulent flows are a necessity in the context of flow control/manipulation towards energy efficiency associated with turbulent skin friction. A clear justification is given by the unaffordable computational requirements for the direct numerical simulation of turbulent flows of industrial relevance, or even canonical flows at very high Reynolds numbers. This means that computationally-cheaper low-dimensional models able to represent the main features of turbulent flows must be employed in flow control investigations.

In this context, the recent success of the resolvent model developed by McKeon & Sharma [6] showing that the interaction of a small subset of resolvent modes driven by linear response-forcing mechanisms can represent the behavior of coherent structures [8], potentially provides a novel low-dimensional manner of describing turbulent flows. This model consists of a gain analysis in Fourier space of the resolvent operator that linearly relates the fluctuating velocity and the nonlinear terms that sustain the turbulence. Also, it differs from other models in its non-empirical construction; it is solely based on the Navier–Stokes equations and the mean flow, which needs to be provided and restricts the allowable resolvent modes. However, the main drawback of the model is that it only provides information on what flow structures are most amplified; it ignores the quantity of nonlinear forcing being amplified. In other words, the resolvent modes needs to be weighted in order to quantitative represent the flow field.

Moarref *et al.* [7] were the first to construct a low-order decomposition based on resolvent modes able to represent the turbulent velocity spectra of a high Reynolds number channel flow. The weightings of the resolvent modes were obtained as the solution of a convex optimization problem, formulated to fit a given direct numerical simulation (DNS) spectra. They showed that although 2 resolvent modes per wavenumber-frequency combination are enough to capture the main features of the turbulent spectra, reconstructions consisting of 12 optimally weighted resolvent modes per wavenumber-frequency combination still present deviation errors of order 20%. In this aspect, the work of Bourguignon [2] reproducing the streamwise energy of a DNS dataset using a modification of the resolvent modes and the proper orthogonal decomposition (POD) of turbulent pipe flow carried out by Duggleby *et al.* [4] are also worth of consideration.

Another important property of this model is that the clear link between resolvent modes and the flow dynamics allows the isolation of specific coherent structures. In this same context, Gómez *et al.* [5] provided further evidence of the feasibility of a low-order decomposition based on the resolvent analysis by explaining the sparsity characteristics of the model, intimately related to low-dimensionality. They showed that the sparse energetically dominant frequencies in turbulent pipe flow observed by Bourguignon *et al.* [3] are caused by a critical layer mechanism [6] as consequence of the discrete treatment of turbulent flows. The link between amplification and energy shown in their numerical experiments suggests that the most amplified resolvent modes may have the largest energy content.

The present work provides the first steps towards a full reconstruction of turbulent flows by means of coupling a DNS solver with the resolvent model. For this purpose, a novel numerical methodology involving Fourier analysis and the projection of response modes onto DNS data has been developed in order to estimate the weights of the resolvent modes and hence, to provide a low-order representation of turbulent flows using the resolvent model.

Numerical Method

A spectral element–Fourier numerical discretization in cylindrical coordinates [1] with a second-order velocity-correction scheme for time integration has been employed to solve the incompressible Navier–Stokes equations in non-dimensional form,

$$\nabla \cdot \hat{\mathbf{u}} = 0 \tag{1}$$

$$\frac{\partial \hat{\mathbf{u}}}{\partial t} + \hat{\mathbf{u}} \cdot \nabla \hat{\mathbf{u}} = -\nabla p + Re^{-1} \nabla^2 \hat{\mathbf{u}} + f_x \tag{2}$$

where Re is the Reynolds number based on the bulk velocity and pipe diameter $D = 2R$, $\hat{\mathbf{u}} = (u, v, w)$ is the velocity vector expressed in cylindrical coordinates (x, r, θ) and p is the modified pressure. A constant streamwise body force f_x acts as a constant streamwise pressure gradient to ensure that the velocity and pressure are streamwise periodic. A (x, r)-domain of length $L = 2\pi D$ is employed and a Fourier discretization is applied in the periodic azimuthal direction. This permits writing the velocity obtained from the DNS as a sum of azimuthal Fourier modes $\hat{\mathbf{v}}_n(x, r, t)$

$$\hat{\mathbf{u}}(x, r, \theta, t) = \sum_{\pm n} \hat{\mathbf{v}}_n(x, r, t) e^{in\theta}. \tag{3}$$

A DNS dataset of pipe flow at $Re = 10000$ consisting on 1200 snapshots equispaced in $T \sim O(50)$ wash-out times has been generated for the present work. Given that the present pipe mean flow obtained from this DNS dataset is one-dimensional, $\mathbf{u_0} = (u_0(r), 0, 0)$, it may appear inefficient to introduce a two-dimensional formulation for a smooth straight pipe flow. However, this is done for two reasons: to make extensive use of equation (3), avoiding significant post-processing of DNS data, and to facilitate the selection of most amplified modes by not exploiting the homogeneity in the axial direction. This means that, as opposed to the original one-dimensional resolvent formulation [6], the axial coordinate x is not Fourier-transformed into an axial wavenumber k, thus the fluctuating velocity and nonlinear terms are functions of both radial and axial coordinates. This two-dimensional treatment is explained in detail next.

A Fourier decomposition of the fluctuating velocity $\mathbf{u} = \hat{\mathbf{u}} - \mathbf{u_0}$ reads

$$\mathbf{u}(x,r,\theta,t) = \sum_{\pm n} \int_{\omega} \mathbf{u}_{n,\omega}(x,r) e^{\mathrm{i}(n\theta - \omega t)} \mathrm{d}\omega + c.c., \qquad (4)$$

where n is the non-dimensional azimuthal wavenumber, $\omega/2\pi$ is the temporal linear frequency and $c.c.$ denotes complex conjugate. The complex conjugate is added because the right hand–side of equation (4) needs to be real. As a consequence, the following symmetries apply in the (n,ω) Fourier modes

$$\begin{aligned}
\mathbf{u}_{n,\omega} &= (u_{n,\omega}, v_{n,\omega}, w_{n,\omega}) && (5)\\
\mathbf{u}_{-n,\omega} &= (u_{n,\omega}, v_{n,\omega}, -w_{n,\omega}) && (6)\\
\mathbf{u}_{n,-\omega} &= (u^*_{n,\omega}, v^*_{n,\omega}, -w^*_{n,\omega}) && (7)\\
\mathbf{u}_{-n,-\omega} &= (u^*_{n,\omega}, v^*_{n,\omega}, w^*_{n,\omega}). && (8)
\end{aligned}$$

In a similar way, the nonlinear convective terms are Fourier-transformed as $\mathbf{f}_{n,\omega} = (\mathbf{u}\cdot\nabla\mathbf{u})_{n,\omega}$. A manipulation of the Navier–Stokes equation (2) with the Fourier decompositions in equation (4) yields the linear relation

$$\mathbf{u}_{n,\omega}(x,r) = \mathcal{H}_{n,\omega}\mathbf{f}_{n,\omega}(x,r), \qquad (9)$$

for each (n,ω) combination. The operator $\mathcal{H}_{n,\omega}$ is known as the resolvent and only depends on the mean flow. The resolvent acts as a transfer function between the fluctuating velocity and the nonlinear terms, in which the nonlinear terms are considered as the forcing that drive the turbulent fluctuations. A singular value decomposition (SVD) of the resolvent operator

$$\mathcal{H}_{n,\omega} = \sum_m \boldsymbol{\psi}_{n,\omega,m}\sigma_{n,\omega,m}\boldsymbol{\phi}^*_{n,\omega,m} \qquad (10)$$

provides an amplification relationship between a set of orthonormal singular response modes $\boldsymbol{\psi}_{n,\omega,m}$ and singular forcing modes $\boldsymbol{\phi}_{n,\omega,m}$ via the magnitude of the corresponding singular value $\sigma_{n,\omega,m}$. Here, the subscript m denotes the order of resolvent mode. To relate this gain analysis to the velocity fields, each Fourier projection of the nonlinear terms is decomposed as a sum of singular forcing modes

$$\mathbf{f}_{n,\omega} = \sum_m \chi_{n,\omega,m}\boldsymbol{\phi}_{n,\omega,m} \qquad (11)$$

where the unknown forcing coefficients $\chi_{n,\omega,n}$ represent the nonlinear interactions sustaining the turbulence. The fluctuating velocity field is then reconstructed as a weighted sum of singular response modes

$$\mathbf{u}(x,r,\theta,t) = \sum_\omega \sum_n \sum_m a_{n,\omega,m}\boldsymbol{\psi}_{n,\omega,m}(x,r)e^{\mathrm{i}(n\theta-\omega t)}, \qquad (12)$$

where the modes complex amplitudes

$$a_{n,\omega,m}e^{-\mathrm{i}\omega t} = \int_{\omega-\Delta\omega/2}^{\omega+\Delta\omega/2} \chi_{n,\omega',m}\sigma_{n,\omega',m}e^{-\mathrm{i}\omega' t}\mathrm{d}\omega' \qquad (13)$$

are defined as the product of the nonlinear forcing and the resolvent amplifications integrated in frequency over a frequency bin $\Delta\omega$ with the purpose of discretizing the integral in frequency. Further details on the two-dimensional resolvent formulation are given by Gómez et al. [5].

As previously discussed, the missing information from the model are the complex amplitudes $a_{n,\omega,m}$ which here are obtained from the DNS dataset. By coupling the DNS solution in equation (3) and the resolvent model in equation (12), we obtain the relation

$$\hat{\mathbf{v}}_n(x,r,t) = \sum_{\pm\omega}\sum_m a_{n,\omega,m}\boldsymbol{\psi}_{n,\omega,m}(x,r)e^{-\mathrm{i}\omega t}, \qquad (14)$$

for each azimuthal wavenumber n. Equation (14) is premultiplied by the complex conjugate of the mode corresponding to frequency η and SVD index q and integrated over the (x,r)-domain Ω

$$\int_\Omega \boldsymbol{\psi}^*_{n,\eta,q}(x,r)\cdot\hat{\mathbf{v}}_n(x,r,t)\mathrm{d}\Omega = \int_\Omega \sum_\omega\sum_m a_{n,\omega,m}\boldsymbol{\psi}^*_{n,\eta,q}(x,r)\cdot\boldsymbol{\psi}_{n,\omega,m}(x,r)e^{-\mathrm{i}\omega t}\mathrm{d}\Omega, \qquad (15)$$

where $\mathrm{d}\Omega = r\mathrm{d}r\mathrm{d}x$. Making use of the orthonormality of the resolvent modes in Ω, the following scalar equation is obtained

$$P_{n,\eta,q}(t) = a_{n,\eta,q}e^{-\mathrm{i}\eta t} + \int_\Omega \sum_{\omega\neq\eta}\sum_{m\neq q} a_{n,\omega,m}\boldsymbol{\psi}^*_{n,\eta,q}(x,r)\cdot\boldsymbol{\psi}_{n,\omega,m}(x,r)e^{-\mathrm{i}\omega t}\mathrm{d}\Omega, \qquad (16)$$

where $P_{n,\omega,m}(t)$ is denoted as the temporal projection coefficients and correspond to the evolution in time of the projection of response modes onto DNS snapshots. The amplitude coefficients $a_{n,\omega,m}$ are obtained by estimating the power spectral density (PSD) of the temporal projection coefficients $P_{n,\omega,w}(t)$ at the corresponding frequency bin $\Delta\omega$. Welch's method is employed for this purpose, which in a simplified manner reads

$$a^*_{n,\omega,m}a_{n,\omega,m} \approx \int_{\omega-\Delta\omega/2}^{\omega+\Delta\omega/2} PSD\left(P_{n,\omega,w}(t)\right)\mathrm{d}\omega. \qquad (17)$$

Note that as a consequence of the symmetries in equation (5)-(8), it follows that

$$\begin{aligned}
a_{n,\omega,m} &= a^*_{-n,-\omega,m} && (18)\\
a_{n,-\omega,m} &= a^*_{-n,\omega,m} && (19)
\end{aligned}$$

thus only modes (n,ω) and $(n,-\omega)$ need to be projected.

This energy-based approach do not recover the phase of the amplitude coefficients $a_{n,\omega,m}$. To obtain a representative phase of the amplitudes, the DNS azimuthal modes are Fourier–transformed in time as

$$\hat{\mathbf{v}}_{n,\omega} = \lim_{T\to\infty}\frac{1}{T}\int_0^T \hat{\mathbf{v}}_n(x,r,t)e^{\mathrm{i}\omega t}\mathrm{d}t \approx \sum_m \chi_{n,\omega,m}\sigma_{n,\omega,m}\boldsymbol{\psi}_{n,\omega,m}(x,r) \qquad (20)$$

in which orthonormality in time is assumed for a value of $T \sim O(50)$ wash-out times. Equation (20) contains $3N$ scalar equations (degrees of freedom in DNS) and m unknowns, thus the problem is solved using a least-squares approach. The pseudo-inverse of a $3N \times m$ matrix $\boldsymbol{\Psi}_{n,\omega}$ whose m rows are the response modes $\boldsymbol{\psi}_{n,\omega,m}$ is computed to obtain

$$\mathcal{X} = \boldsymbol{\Psi}^{+}_{n,\omega} \hat{\mathbf{v}}_{n,\omega} \tag{21}$$

in which the $m \times 1$ vector $\mathcal{X}$ contains a least-squares approximation of $\chi_{n,\omega,m}\sigma_{n,\omega,m}$. We highlight the subtle distinction between coefficients $a_{n,\omega,m}$ obtained by projections and the coefficients $\chi_{n,\omega,m}\sigma_{n,\omega,m}$ computed via least-squares. The energy contained in each frequency bin $\Delta\omega$ is taken into account for the obtention of the $a_{n,\omega,m}$ coefficients while the $\chi_{n,\omega,m}\sigma_{n,\omega,m}$ are only useful for providing a representative phase for the amplitudes. And thus, the validity of the relation $a_{n,\omega,m} \simeq \chi_{n,\omega,m}\sigma_{n,\omega,m}\Delta\omega$ depends on the quality of the least-square approximation.

Results

Figure 1(a) present a comparison between the principal resolvent amplification $\sigma_{n,w,1}$ obtained via the SVD of the resolvent in equation (10) and Figure 1(b) shows the amplitude coefficients $a_{n,w,1}$ recovered by the projection of the corresponding principal resolvent modes onto the DNS dataset.

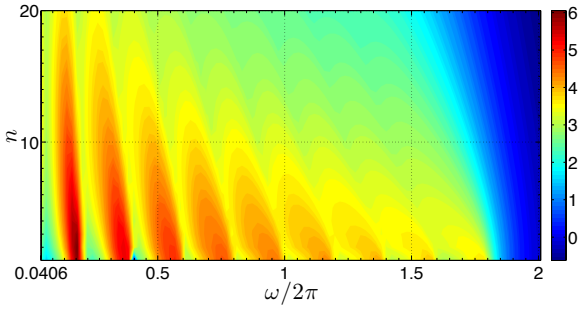

(a) $\log_{10}(\sigma_{n,w,1})$

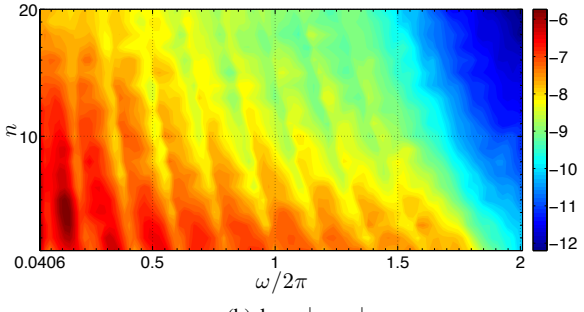

(b) $\log_{10}|a_{n,w,1}|$

Figure 1. Distribution of (a) resolvent amplification $\sigma_{n,w,1}$ (b) amplitude $a_{n,w,1}$ in the energetically active subset of azimuthal wavenumbers n and frequencies $\omega/2\pi$ for the first singular vector $m = 1$ at $Re = 10000$.

A clear correspondence between amplification and energy is observed. The sparsity of amplification in frequency is transferred to the energy, although the nonlinear terms play a major role in smoothing the sparsity, consistently with the findings of Gómez *et al.* [5]. In order to assess the importance of the most amplified modes, a comparison between the azimuthal modal energies obtained from this model and the ones provided by the DNS dataset has been carried out. The energy of each azimuthal mode from the DNS is defined as

$$E_n = \lim_{T\to\infty} \frac{1}{T} \int_0^T \frac{1}{2A} \int_\Omega \hat{\mathbf{v}}^*_n(x,r,t) \cdot \hat{\mathbf{v}}_n(x,r,t) \mathrm{d}\Omega \mathrm{d}t \tag{22}$$

where A is the area of the (x,r)-domain Ω. Following the resolvent decomposition in equation (12), the modal energies can be written is term of the recovered amplitudes as

$$E_n = \frac{1}{2A} \sum_{\pm\omega} \sum_m a^*_{n,\omega,m} a_{n,\omega,m} + a^*_{-n,\omega,m} a_{-n,\omega,m} \,. \tag{23}$$

Figure 2 shows the comparison between DNS modal energies and the energy obtained by means of the projection methodology using $m = 1$ to $m = 10$ of the most amplified response modes $\boldsymbol{\psi}_{n,\omega,m}(x,r)$ per frequency, employing 98 equispaced frequency bins. We observe that the trend of the energy cascade is recovered and that 55.5% of the energy is recovered by the sum of the 10 most amplified response modes per frequency, among which the principal response mode $m = 1$ is the most energetic and recovers 22.3% of the total energy. Compared to the results of Duggleby *et al.* [4] at $Re = 4300$ in which the most energetic POD mode for each (k,n) combination contains $O(1\%)$ of the total energy, the sum of principal response mode $m = 1$ for each (k,n) *and all frequencies* is of order $O(3\%)$. Moreover, the sparsity in Figure 1(b) plays a major role in the energy distribution, e.g., the mode $(n,\omega,m) = (4, 0.87, 1)$ *alone* contains 0.4% of the total energy, which would be similar to the energy contained in the corresponding POD mode at the present value of Reynolds number $Re = 10000$.

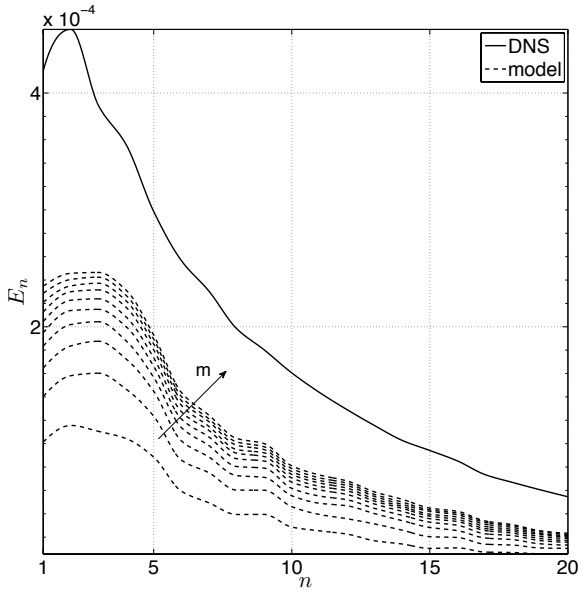

Figure 2. Modal energies E_n in the energetically active subset of azimuthal wavenumbers n for $m = 1$ to $m = 10$ most amplified singular vectors at $Re = 10000$.

Note that the phase information of the amplitudes coefficients is not required for the modal energy calculation. An example of phase recovery by least-squares approximation of a mode $\hat{\mathbf{v}}_{\mathbf{n},\omega}(\mathbf{x},\mathbf{r})$ is shown in Figure 3, in which the first 100 resolvent modes are employed to reconstruct a Fourier mode from the DNS. We observe that the absence of modes presenting high axial wavenumber prevents an exact reconstruction. Nevertheless, increasing m or using a reconstruction based on (k,n,ω,m)

rather than (n,ω,m) could overcome this constraint at the cost of higher DNS post-processing.

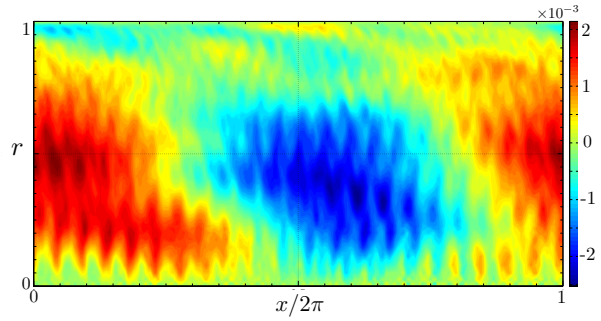

(a) DNS: $\Re\left(\hat{\mathbf{v}}_{\mathbf{n},\omega}(\mathbf{x},\mathbf{r})\right)$

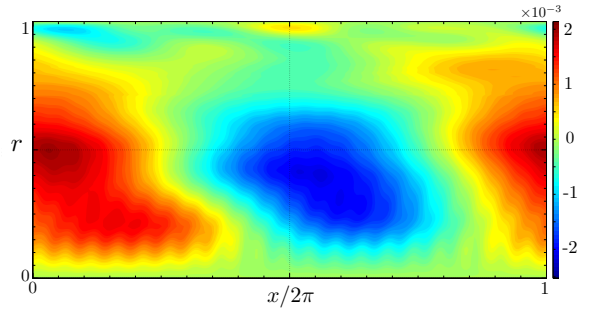

(b) Reconstruction: $\Re\left(\sum_{m=1}^{100} a_{n,\omega,m}\boldsymbol{\Psi}_{n,\omega,m}(x,r)\right)$

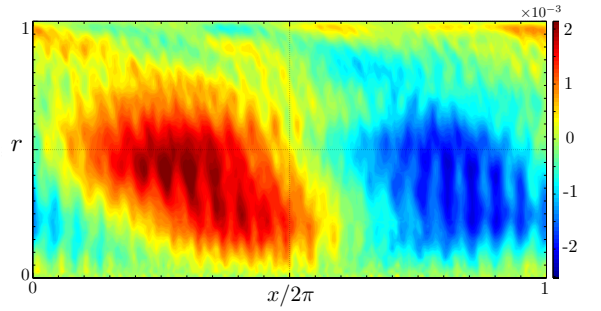

(c) DNS: $\Im\left(\hat{\mathbf{v}}_{\mathbf{n},\omega}(\mathbf{x},\mathbf{r})\right)$

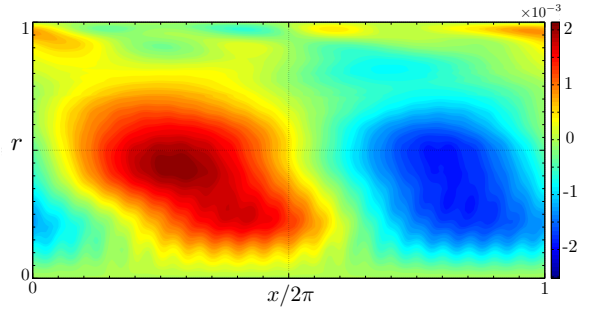

(d) Reconstruction: $\Im\left(\sum_{m=1}^{100} a_{n,\omega,m}\boldsymbol{\Psi}_{n,\omega,m}(x,r)\right)$

Figure 3. Contours of the (a) real and (c) imaginary streamwise velocity of $\hat{\mathbf{v}}_{n,\omega}(x,r)$ modes with $n=2$ and $\omega/2\pi=0.182$ and (b) real and (d) imaginary streamwise velocity of the reconstruction using resolvent modes

The error of this least-squares approximation $e_{n,\omega}$ is shown in Figure 4. Despite only 3 modes are required to represent the Fourier-transformed DNS mode with a 10% error, employing 100 modes reduces the error to only 3%. This is consistent with the diminishing return by employing more resolvent modes observed by Moarref *et al.* [7].

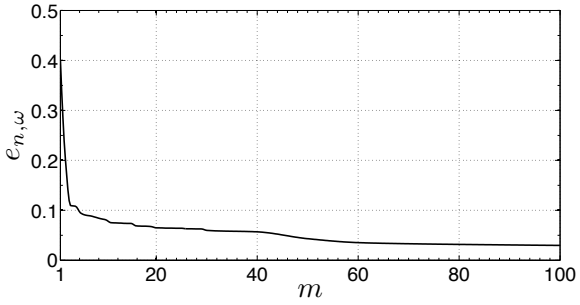

Figure 4. Least-squares approximation error against the number of resolvent modes m employed in the reconstruction.

Conclusions

The present results provide further evidence that the most amplified modes in the resolvent analysis carry the largest energy content and that a small subset of the weighted modes using the present approach can represent general trends of turbulent flows. It is suggested that, if the sparsity in energy is exploited, the present resolvent model could be competitive in a energy-based context against POD analysis with the additional advantage of isolating specific dynamics, which is highly desirable for flow control. Future steps include the reconstruction of the turbulent velocity spectra.

Acknowledgements

The authors acknowledge financial support from the Australian Research Council through the ARC Discovery Project DP130103103, and from Australia's National Computational Infrastructure via Merit Allocation Scheme Grant D77.

References

[1] Blackburn, H. M. and Sherwin, S., Formulation of a Galerkin spectral element–Fourier method for three-dimensional incompressible flows in cylindrical geometries, *J. Comput. Phys.*, **197**, 2004, 759–778.

[2] Bourguignon, J. L., *Models of turbulent pipe flow*, Ph.D. thesis, California Institute of Technology, 2013.

[3] Bourguignon, J.-L., Tropp, J., Sharma, A. S. and McKeon, B. J., Compact representation of wall-bounded turbulence using compressive sampling, *Phys. Fluids*, **25**, 2014, 015109.

[4] Duggleby, A., Ball, K., Paul, M. and Fischer, P., Dynamical eigenfunction decomposition of turbulent pipe flow, *Journal of Turbulence*, **8**, 2007, 1–24.

[5] Gómez, F., Blackburn, H. M., Murray, R., McKeon, B. J., Luhar, M., Moarref, R. and Sharma, A. S., On the origin of frequency sparsity in direct numerical simulation of turbulent pipe flow, *Submitted to Phys. Fluids*.

[6] McKeon, B. J. and Sharma, A. S., A critical layer framework for turbulent pipe flow, *J. Fluid Mech.*, **658**, 2010, 336–382.

[7] Moarref, R., Jovanović, M., Tropp, J., Sharma, A. and McKeon, B., A low-order decomposition of turbulent channel flow via resolvent analysis and convex optimization, *Physics of Fluids*, **26**, 2014, 051701.

[8] Sharma, A. S. and McKeon, B. J., On coherent structure in wall turbulence, *J. Fluid Mech.*, **728**, 2013, 196–238.